Indian J Phys (June 2014) 88(6):547–556
DOI 10.1007/s12648-014-0449-y

ORIGINAL PAPER

Vibrational, structural and hydrogen bonding analysis of *N*′-[(E)-4-Hydroxybenzylidene]-2- (naphthalen-2-yloxy) acetohydrazide: combined density functional and atoms-in-molecule based theoretical studies

A K Srivastava[1], B Narayana[2], B K Sarojini[3] and N Misra[1]*

[1]Department of Physics, University of Lucknow, Lucknow 226007, Uttar Pradesh, India

[2]Department of Studies in Chemistry, Mangalore University, Mangalagangotri 574199, Karnataka, India

[3]Department of Chemistry, P A College of Engineering, Mangalore 574153, Karnataka, India

Received: 30 October 2013 / Accepted: 15 January 2014 / Published online: 30 January 2014

Abstract: DFT-B3LYP/6-311G calculations are performed on *N*′-[(E)-4-Hydroxybenzylidene]-2-(naphthalen-2-yloxy) acetohydrazide to explore its structural and vibrational properties. A good correlation is shown between experimental and calculated bond lengths and vibrational frequencies. Atoms-in-molecule analysis is employed for detection and characterization of an intra-molecular hydrogen bonding interaction present in molecule. The effect of hydrogen bonding on structural as well as vibrational properties is also discussed. Natural population analysis, highest occupied molecular orbital–lowest unoccupied molecular orbital and molecular electrostatic potential plots along with various electronic and thermodynamic parameters are presented at the same level of theory.

Keywords: Hydrazones; DFT; AIM; Normal modes; FTIR

PACS Nos.: 31.15.A-; 82.30.Rs; 87.15.A-

1. Introduction

Schiff base hydrazones are now well recognized for their pharmacological importance and biological activities. Hydrazones and its derivatives have been demonstrated to possess antimicrobial, antitubercular [1–5] and antidiabetic agents [6]. They have strong coordinating ability towards different metal ions [7]. In addition, aroyl hydrazones and their mode of chelation with transition metal ions present in the living system have been of significant interest [8, 9]. The chemical stability of hydrazones and their high melting point have recently made them attractive as prospective new material for opto-electronic applications [10]. Phenyl hydrazones exhibit a series of good organic nonlinear optical properties [11, 12]. Hydrazide-hydrazones are very significant in the way they can be used for synthesizing many effective drugs [13]. A literature survey reveals a number of studies performed on in vivo and in vitro metabolism of hydrazide-hydrazones [14–17]. It seems quite interesting to perform a theoretical investigation on such biologically active molecules. The present work deals with the study of a hydrazide-hydrazone viz. *N*′-[(E)-4-Hydroxybenzylidene]-2-(naphthalen-2-yloxy) acetohydrazide with empirical chemical formula $C_{19}H_{16}N_2O_3$ using density functional theory (DFT).

DFT has established itself as an efficient tool for the study of structural and vibrational properties of biomolecules [18, 19]. It provides sufficient confidence about the results when incorporated by proper exchange–correlation functional. A hybrid type functional, B3LYP in which Becke three parameter exchange is combined with Lee, Yang and Parr's correlation, has become very popular because of its compromise with accuracy and computational cost. We have used B3LYP functional in conjunction with 6-311G basis set to calculate structural and vibrational properties of a hydrazide

Electronic supplementary material The online version of this article (doi:10.1007/s12648-014-0449-y) contains supplementary material, which is available to authorized users.

*Corresponding author, E-mail: neerajmisra11@gmail.com

molecule. For comparison, we have included experimental X-ray crystallographic parameters and FTIR spectra and shown a correlation between experimental and theoretical results. Various molecular properties, electronic and thermodynamic, are also calculated, giving an estimation of chemical reactivity and reaction paths. Natural population analysis (NPA), highest occupied molecular orbital (HOMO)–lowest unoccupied molecular orbital (LUMO) and molecular electrostatic potential (MESP) surfaces are used to discuss electron density distribution and resulting intra-molecular charge transfers.

It is widely accepted that hydrogen bonds play a key role in determining the structures, properties and functions of biomolecules [20]. Bader's atoms-in-molecule (AIM) theory [21] can successfully be applied for the study of hydrogen bonding. The AIM theory efficiently describes the nature and strength of various types of hydrogen-bonded interactions. One of the advantages of the AIM theory is its ability to provide information on the change in electron density distribution as a result of either bond formation or complex formation. The basis set reliability and stability in the values of AIM parameters have been studied and it was found that they are almost independent of basis set in case of used functional B3LYP in DFT [22]. However, it has been noticed that B3LYP functional underestimates weak intramolecular interactions as well as charge transfer effects [23–25].

2. Methodology

All the DFT calculations were performed with the help of Gaussian 09 software package [26] using a hybrid functional B3LYP and employing 6-311G as a basis set. Initial geometry was adopted from crystal structure of the molecule under study reported by Kant et al. [27]. This geometry was fully optimized without any constraint in potential energy surface (PES). AIM analysis was performed by AIMAll program [28]. NPA analysis was carried out by NBO 3.1 program [29] as implemented in Gaussian 09. The potential energy distribution (PED) for various vibrational modes was calculated by VEDA 4 program [30]. All the relevant plots and graphics were created by Gauss View 5.0 program [31].

The compound, *N*′-[(E)-4-Hydroxybenzylidene]-2-(naphthalen-2-yloxy) acetohydrazide, was purchased from Sigma Aldrich with a purity of 98 % and used as such without further purification for spectroscopic processing. The FTIR spectrum was recorded in a Shimadzu- spectrometer (Model Prestige 21) with normal resolution of 4 cm^{-1} in the region 400–4,000 cm^{-1} with sample in KBr pellet.

3. Results and discussions

3.1. Optimized structure and hydrogen bonding

The optimized geometry of *N*′-[(E)-4-Hydroxybenzylidene]-2-(naphthalen-2-yloxy) acetohydrazide is shown in Fig. 1 with atomic labelling. Supplementary Table S1 lists bond-lengths, bond-angles and important dihedrals of optimized structure. The optimized parameters show close resemblance with crystallographic data which are also presented in Table S1 for a comparison. The experimental and calculated bond-lengths are correlated linearly as $y = 0.7342\ x + 0.387$ as shown in Fig. 2 with a correlation coefficient of 0.987. Furthermore, the calculated structural parameters agree well with the values reported in literature [32]. The maximum C–C bond length (among others), 1.4344 A° in naphthalene ring system agrees with reported value of 1.42 A°. The calculated C37–C36–C27 bond angle, 119.38° shows excellent agreement with reported value of 119.4°. In acetohydrazide fragment, C16–C17 and C16–O21 bond lengths are 1.5216 A° and 1.2402 A° respectively while the respective bonds in acetone are reported to be 1.520 and 1.214 A°. Thus, the C–O bond is affected by the presence of hydrazine group but not C–C bond.

AIM calculations show an intra-molecular hydrogen bonding interaction between O22 and H39 of acetohydrazide fragment. In AIM theory, the existence of hydrogen bond follows Koch and Popelier criterion [33] which requires an existence of bond critical point (BCP) for the 'proton (H)…acceptor (A)' contact. The value of electron density (ρ) should lie in the range 0.002–0.040 a.u. and corresponding Laplacian ($\nabla^2\rho$) should be within the range 0.024–0.139 a.u. These topological parameters calculated at BCP of O22. H39 along with geometrical parameters of H-bond are listed in Table 1. The three types of H-bond are characterized on the basis of topological parameters. According to Rozas et al. [34], the characterization demands at BCP that $\nabla^2\rho < 0$ and $H < 0$ for strong H-bond of covalent nature, $\nabla^2\rho > 0$ and $H < 0$ for medium H-bond of partially covalent nature and $\nabla^2\rho > 0$ and $H > 0$ for weak H-bond of electrostatic character. From Table 1, it is apparent that Laplacian of charge density is positive, $\nabla^2\rho = 0.1056$ suggesting the interaction to be weak in nature. For strong covalent interactions, this value is found to be negative and small in magnitude, for example, that in [Mn(III) porphyrin]Cl-trimethoprim complex ($\nabla^2\rho = -0.0786$ a.u.) [35] and bis-dithiazolyl dimers [36]. The energy of interaction has been estimated by $E_{int} = ½\ (V)$ at BCP as proposed by Espinosa et al. [37]. The calculated interaction energy of O22..H39 is 5.835 kcal/mol. The stretching in N15-H39 bond length 1.0155 A° from 0.868 A° suggests the presence of H-bond.

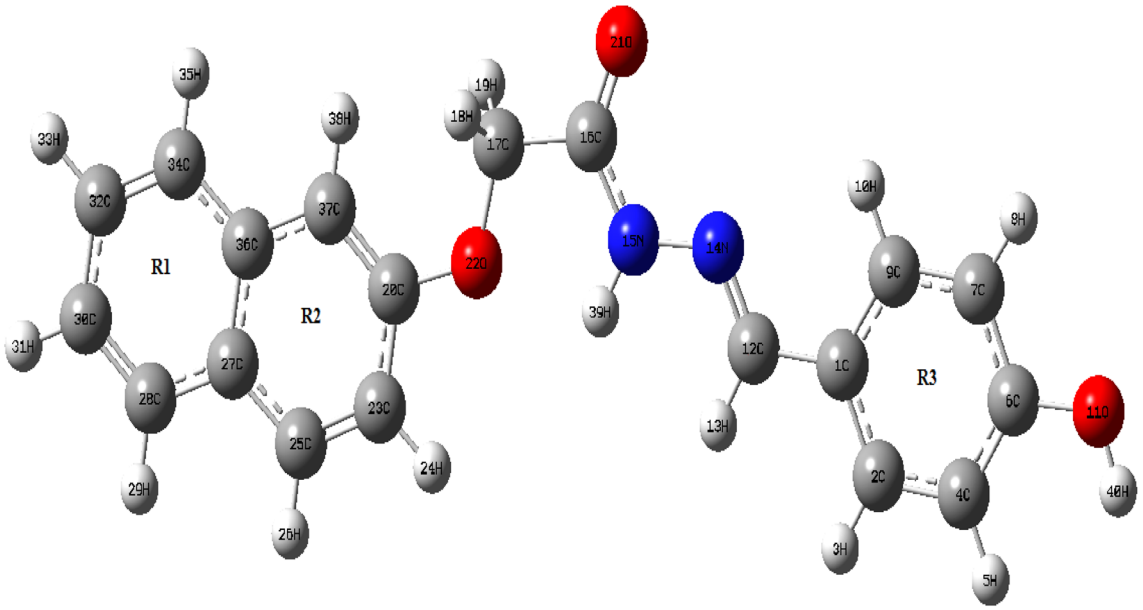

Fig. 1 Optimized geometry of *N′*-[(E)-4-Hydroxybenzylidene]-2-(naphthalen-2-yloxy) acetohydrazide at B3LYP/6-311G level

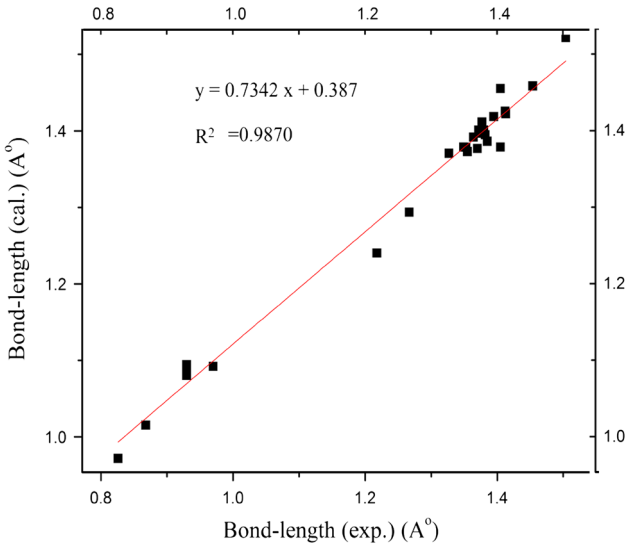

Fig. 2 Correlation between calculated and experimental bond lengths

The geometry of this H-bond viz. length of O22..H39, 2.077 A° and angle O22..H39–N15, 108.9° further give an indication of weak interaction [38].

3.2. Normal mode analysis and FTIR

The vibrational analysis of studied molecule has been performed at the same level of theory. All the calculated frequencies corresponding to the optimized geometry are found to be real. Thus the optimized geometry corresponds to a true minimum in the PES. Calculated frequencies are uniformly scaled with a factor of 0.96 [39] to compensate the errors due to neglect of anharmonic terms by the present theoretical model. All the vibrational modes are properly assigned on the basis of PED. Table 2 lists calculated frequencies (unscaled as well as scaled), intensities, FTIR frequencies and assignments of all the normal modes up to 400 cm^{-1}. Figure 3 gives a visual comparison of experimental and simulated spectra from 400 up to 3,500 cm^{-1}. The investigated molecule contains substituted naphthalene (R1 and R2) and benzene (R3) rings linked by acetohydrazide fragment (–CH_2–CO–NH–N=).

Pure C–H stretching frequencies of the rings are calculated in the range 3,086–3,026 cm^{-1}. The maximum C–H stretching of 3,086 cm^{-1} belongs to R3 ring. The corresponding values reported in literature lie in between 3,000 and 3,100 cm^{-1} with medium or weak intensities [40]. The calculated frequencies 1,602 and 1,576 cm^{-1} correspond to pure C–C stretching of R1 and R2 while C–C stretching vibrations mixed with other modes are found in lower frequency region. For R3 ring, a strong absorption can be seen at

Table 1 Topological and geometrical parameters for intra-molecular hydrogen bond, N15–H39..O22

Topological parameters[a]	Geometrical parameters[b]
Electron density (ρ) = 0.0202	N15–H39 = 1.0155
Laplacian ($\nabla^2\rho$) = 0.1056	O22…H39 = 2.0770
Kinetic energy density (G) = 0.0225	N15…O22 = 2.5912
Potential energy density (V) = −0.0186	N15–H39…O22 = 108.94
Total energy density (H) = 0.0039	

[a] All parameters in a.u

[b] Bond length in A° and bond angle in deg

Table 2 Vibrational analysis at B3LYP/6-311G level (corresponding FTIR values are also included)

Freq.	Sc. freq.	IR int.	FTIR	PED %[a] with vibrational assignments[b] (mode)
3,699	3,551	68.7	3,261	R3[100 % ν $OH(S_1)$]
3,492	3,352	34.5	3,157	100 % ν $NH(S_2)$
3,215	3,086	5.6		R3[46 % ν $CH(S_5)$ + 53 % ν $CH(S_6)$]
3,203	3,074	12.5		R2[88 % ν $CH(S_7)$ + 10 % ν $CH(S_8)$]
3,199	3,071	2.6		R3[53 % ν_s $CH(S_5)$ + 46 % ν_{as} $CH(S_6)$]
3,197	3,069	7.6		R2[90 % ν $CH(S_{13})$]
3,195	3,067	50.8		R1[46 % ν $CH(S_{10})$ + 33 % ν $CH(S_{11})$]
3,179	3,051	39.8		R1[15 % ν_{as} $CH(S_9)$ + 26 % ν_{as} $CH(S_{10})$ + 35 % ν_s $CH(S_{11})$ + 22 % ν_s $CH(S_{12})$]
3,173	3,046	24.7		R3[58 % ν $CH(S_3)$ + 41 % ν $CH(S_4)$]
3,170	3,043	9.5		R2[10 % ν_{as} $CH(S_7)$ + 85 % ν_s $CH(S_8)$]
3,163	3,036	0.7		R1[44 % ν $CH(S_9)$ + 38 % ν $CH(S_{12})$]
3,158	3,031	5.3		R1[30 % ν_s $CH(S_9)$ + 17 % ν_{as} $CH(S_{10})$ + 20 % ν_s $CH(S_{11})$ + 32 % ν_{as} $CH(S_{12})$]
3,153	3,026	23.5		R3[42 % ν_{as} $CH(S_3)$ + 58 % ν_s $CH(S_4)$]
3,078	2,954	12.7	2,927	50 % ν_s $C_{17}H_{18}(S_{15})$ + 50 % ν_{as} $C_{17}H_{19}(S_{16})$
3,029	2,907	62.7		50 % ν_s $C_{17}H_{18}(S_{15})$ + 50 % ν_s $C_{17}H_{19}(S_{16})$]
3,025	2,904	311.3	2,850	100 % ν $C_{12}H_{13}(S_{14})$
1,693	1,625	59.9	1,656	77 % ν $O_{21}C_{16}(S_{17})$
1,669	1,602	79.5	1,604	R2[16 % ν_{as} $CC(S_{19})$ + 10 % ν_s $CC(S_{22})$ + 19 % ν_{as} $CC(S_{31})$ + 13 % ν_s $CC(S_{33})$]
1,655	1,588	71.2		19 % ν $N_{14}C_{12}(S_{18})$ + R3[20 % ν $CC(S_{23})$ + 11 % ν $CC(S_{24})$]
1,651	1,584	57.6		36 % ν $N_{14}C_{12}(S_{18})$ + 13 % τ $HCN(S_{56})$ + R3[15 % ν $CC(S_{26})$]
1,642	1,576	2.8		R2[19 % ν_s $CC(S_{19})$ + 12 % ν_{as} $CC(S_{22})$] + R1[16 % ν_s $CC(S_{20})$ + 16 % ν_{as} $CC(S_{21})$]
1,615	1,550	45.5	1,556	R2[12 % ν_{as} $CC(S_{22})$] + R1[17 % ν $CC(S_{28})$ + 12 % δ_i $CCC(S_{42})$]
1,614	1,549	333.2		R3[25 % ν $CC(S_{25})$]
1,584	1,520	15.2	1,512	14 % ν $N_{15}C_{16}(S_{29})$ + 57 % σ $HNN(S_{44})$
1,554	1,491	274.3		R3[16 % δ_i $HCC(S_{45})$ + 15 % δ_o $HCC(S_{46})$ + 10 % δ_o $HCC(S_{47})$ + 11 % δ_o $HCC(S_{48})$]
1,529	1,467	14.6	1,465	74 % σ $HCH(S_{58})$
1,513	1,452	108.8		R2[11 % δ_i $HCC(S_{49})$ + 14 % δ_o $HCC(S_{50})$] + R1[15 % δ_i $HCC(S_{53})$ + 11 % δ_i $HCC(S_{54})$]
1,491	1,431	4.7	1,438	R1[12 % ν $CC(S_{31})$ + 22 % δ_i $HCC(S_{52})$ + 10 % δ_i $HCC(S_{53})$]
1,473	1,414	2.5		R3[17 % ν_{as} $CC(S_{23})$ + 10 % ν_s $CC(S_{24})$ + 12 % δ_o $HCC(S_{46})$ + 14 % δ_i $HCC(S_{47})$]
1,420	1,363	48.7	1,384	R2[12 % ν $CC(S_{19})$ + 15 % ν $CC(S_{22})$ + R1[12 % δ_i $CCC(S_{42})$]
1,410	1,353	15.0		R2[10 % δ_o $HCC(S_{49})$ + 10 % δ_i $HCC(S_{55})$] + 21 % σ $HCN(S_{56})$
1,409	1,352	23.5		31 % σ $HCN(S_{56})$
1,400	1,344	9.5		R1[15 % ν $CC(S_{21})$] + 13 % τ_i $HCOC(S_{92})$ + 21 % τ_o $HCOC(S_{93})$
1,392	1,336	4.6		R1[18 % ν $CC(S_{21})$] + 12 % τ_o $HCOC(S_{92})$ + 19 % τ_i $HCOC(S_{93})$
1,382	1,326	47.0	1,309	R3[16 % δ_i $HOC(S_{43})$ + 16 % δ_i $HCC(S_{45})$ + 26 % δ_i $HCC(S_{48})$]
1,347	1,293	12.2	1,278	R3[13 % ν_{as} $CC(S_{24})$ + 19 % ν_s $CC(S_{26})$]
1,308	1,255	8.3	1,257	R1[10 % δ_i $CCC(S_{42})$ + 10 % δ_o $HCC(S_{51})$ + 12 % δ_o $HCC(S_{54})$] + R2[10 % δ_o $HCC(S_{55})$ + 10 % δ_o $CCC(S_{71})$]
1,302	1,249	51.0		R1[10 % ν_{as} $CC(S_{33})$ +10 % δ_o $HCC(S_{51})$] + R2[20 % δ_i $HCC(S_{50})$]
1,288	1,236	41.2		R3[10 % ν_{as} $CC(S_{25})$ + 39 % ν $OC(S_{35})$ + 12 % δ_i $HCC(S_{46})$]
1,276	1,224	150.0		15 % ν $N_{15}C_{16}(S_{29})$ + 17 % ν_s $C_{12}C_1(S_{34})$ + 12 % τ $HNN(S_{44})$ + 10 % τ $HCN(S_{56})$
1,264	1,213	42.4	1,215	18 % ν $N_{15}C_{16}(S_{29})$ + 16 % ν_{as} $C_{12}C_1(S_{34})$ + 13 % ν_{as} $C_{16}C_{17}(S_{38})$ + 10 % ω $HNN(S_{44})$
1,251	1,200	3.2		67 % τ $HCO(S_{57})$ + 23 % τ_o $HCOC(S_{93})$

Table 2 continued

Freq.	Sc. freq.	IR int.	FTIR	PED %[a] with vibrational assignments[b] (mode)
1,248	1,198	113.6	1,184	R1[23 % ν_s CC(S_{32}) + 12 % ν_{as} CC(S_{33}) + 12 % δ_i HCC(S_{52}) + 12 % δ_o HCC(S_{53})]
1,213	1,164	9.3	1,166	R3[21 % δ_i HCC(S_{45}) + 25 % δ_i HCC(S_{46}) +12 % δ_i HCC(S_{47}) + 13 % δ_o HCC(S_{48})]
1,209	1,160	182.1		R1[11 % ν_{as} CC(S_{33}) + 15 % δ_o HCC(S_{54})] + 15 % ν OC(S_{37}) + R2[21 % δ_i HCC(S_{55})]
1,203	1,154	73.2		R1[18 % δ_o HCC(S_{51}) + 25 % δ_i HCC(S_{52}) + 14 % δ_o HCC(S_{53})]
1,186	1,138	1.9		R2[13 % ν_s CC(S_{19}) + 29 % δ_i HCC(S_{49}) + 17 % δ_o HCC(S_{50})] + R1[12 % ν_{as} CC(S_{20})]
1,179	1,131	348.7	1,120	R3[15 % ν_{as} CC(S_{27}) + 44 % δ_o HOC(S_{43}) + 16 % δ_i HCC(S_{47})]
1,156	1,109	67.7		R1[10 % δ_o CCC(S_{42})] + R2[14 % δ_o HCC(S_{49})]
1,141	1,095	21.6	1,074	R3[13 % ν_{as} CC(S_{23}) + 12 % ν_s CC(S_{24}) + 10 % δ_o HOC(S_{43}) + 10 % δ_o HCC(S_{47}) + 13 % δ_i HCC(S_{48})]
1,094	1,050	116.5		59 % ν_s NN(S_{36}) + 10 % ν_{as} $C_{16}C_{17}$(S_{38})]
1,047	1,005	1.1	1,006	R1[40 % ν CC(S_{28})]
1,046	1,004	0.5		31 % τ HCO(S_{57}) + 39 % τ_i HCOC(S_{92}) + 17 % τ_o OCNC(S_{111})
1,039	997	0.4		R3[40 % δ_i CCC(S_{64}) + 26 % δ_i CCC(S_{65}) + 15 % δ_o CCC(S_{66})]
1,033	991	51.5		44 % ν $O_{17}C_{22}$(S_{39})
1,024	983	0.1		R1[23 % τ_i HCCC(S_{87}) + 31 % τ_o HCCC(S_{88}) + 15 % τ_i HCCC(S_{89}) + 13 % τ_i CCCC(S_{106})]
1,019	978	3.9		R3[16 % τ_i HCCC(S_{82}) + 60 % τ_o HCCC(S_{83})]
1,005	964	18.5	964	R3[10 % τ_o HCCC(S_{80})] + 74 % τ_o HCNN(S_{91})]
997	957	3.7		R2[10 % τ_o HCCC(S_{84})] + R1adjR2[32 % τ_i HCCC(S_{85})] + R1[14 % τ_i HCCC(S_{86}) + 12 % τ_i HCCC(S_{89})]
994	954	120.5		10 % ν_{as} $N_{15}C_{16}$(S_{29}) + 15 % ν_{as} $O_{17}C_{22}$(S_{39}) + 10 % τ OCN(S_{59}) + 11 % ρ $C_{16}N_{15}N_{14}$(S_{68}) + 10 % σ $N_{15}N_{14}C_{12}$(S_{74})
982	942	7.4		R2[19 % τ_o HCCC(S_{84}) +R1adjR2[24 % τ_i HCCC(S_{85})] + R1[14 % τ_o HCCC(S_{86}) + 15 % τ_i HCCC(S_{87}) + 11 % τ_o HCCC(S_{89})]
951	912	0.7	914	R3[43 % τ_i HCCC(S_{80}) + 16 % τ_o HCCC(S_{81}) + 20 % τ_i CCCC(S_{99})]
931	893	1.0		14 % ν_{as} OC(S_{37}) + R2[11 % δ_o CCO(S_{40})] + R1[11 % δ_i CCC(S_{67})]
905	868	29.8		R1[16 % τ_i HCCC(S_{86}) + 14 % τ_o HCCC(S_{88}) + 12 % τ_o HCCC(S_{89}) + 18 % τ_i HCCC(S_{90})]
879	843	7.5	842	R1[11 % τ_o HCCC(S_{87}) + 42 % τ_i HCCC(S_{90})] + R2[12 % τ_o CCOC(S_{113})]
873	838	69.2		R3[57 % τ_i HCCC(S_{82}) + 25 % τ_i HCCC(S_{83})]
869	834	31.1		R3[13 % ν_s CC(S_{25}) + 13 % ν_s CC(S_{27}) + 24 % δ_i CCC(S_{66})]
840	806	10.1	819	R2[35 % τ_i HCCC(S_{84}) +R1adjR2[26 % τ_i HCCC(S_{85})] + R1[11 % τ_i HCCC(S_{89})]
828	794	31.1		R3[23 % τ_i HCCC(S_{80}) + 60 % τ_i HCCC(S_{81})]
806	773	28.4		R3[14 % ν_{as} CC(S_{27}) + 23 % ν_{as} OC(S_{35}) + 20 % δ_i CCC(S_{41})]
785	753	10.5		R1[11 % ν_s CC(S_{32}) + 29 % δ_i CCC(S_{63})] + R2[11 % δ_o CCO(S_{40})]
776	744	0.6	748	R1[16 % τ_i HCCC(S_{86}) + 27 % τ_i HCCC(S_{87}) + 30 % τ_i HCCC(S_{88}) + 13 % τ_i HCCC(S_{89})]
768	737	28.6		R1[10 % τ_i HCCC(S_{90}) + 21 % τ_o CCCC(S_{97}) + 21 % τ_i CCCC(S_{101}) + 21 % τ_i HCCC(S_{106})]
763	732	1.7		R2[19 % δ_i CCC(S_{61})] + R1[11 % δ_i CCC(S_{67})] + 13 % τ $C_{16}C_{17}O_{22}$(S_{77})
737	707	58.3	713	R3[18 % τ_o CCCC(S_{98}) + 19 % τ_o CCCC(S_{99}) + 10 % τ_i CCCC(S_{100}) + 12 % τ_o OCCC(S_{112}) + 14 % τ_i CCCC(S_{114})]
709	680	6.6	684	88 % τ_i HNNC(S_{79})
698	670	89.9		15 % % ν_{as} $C_{16}C_{17}$(S_{38}) + 18 % σ OCN(S_{59}) + 11 % τ $C_{16}N_{15}N_{14}$(S_{68})
666	639	24.5	644	R3[16 % δ_o CCC(S_{41}) + 19 % δ_o CCC(S_{64}) + 27 % δ_i CCC(S_{65})]
655	628	5.7		R2[19 % τ_o HCCC(S_{84}) + 36 % τ_i CCOC(S_{113})]
601	576	5.3	597	R1[10 % δ_i CCC(S_{63})] + 71 % τ_i OCNC(S_{111})

Table 2 continued

Freq.	Sc. freq.	IR int.	FTIR	PED %[a] with vibrational assignments[b] (mode)
598	574	0.4		R3[11 % ν_s OC(S_{35}) + 16 % δ_o CCC(S_{66})] + 10 % τ $N_{14}C_{12}C_1$(S_{60})
546	524	1.4	530	R1[35 % τ_o CCCC(S_{97}) + 19 % τ_i CCCC(S_{101}) + 10 % τ_i HCCC(S_{106})]
544	522	19.5		R3[10 % τ_o HCCC(S_{80}) + 22 % τ_o OCCC(S_{112}) + 17 % τ_o CCCC(S_{114})]
523	502	0.2		R1[12 % ν_s CC(S_{32}) + 18 % δ_i CCC(S_{62})] + R1adjR2[10 % δ_i CCC(S_{70})] + R2[14 % δ_i CCC(S_{71})]
499	479	15.0		R2[13 % δ_i CCC(S_{61}) + 12 % δ_o CCO(S_{69})] + 12 % ω $C_{20}O_{22}C_{17}$(S_{75})
493	473	19.2	472	R2[10 % τ_o CCCO(S_{95}) + 23 % τ_i CCCC(S_{105}) + 17 % τ_i CCOC(S_{113})] + R1[14 % τ_i CCCC(S_{106})]
463	444	2.8		17 % σ OCN(S_{59}) + 22 % τ $C_{12}C_1C_2$(S_{72}) + 11 % σ NNC(S_{74}) + R3[16 % δ_o OCC(S_{73})]
438	420	0.1		R3[10 % τ_o HCCC(S_{81}) + 12 % τ_i CCCC(S_{98}) + 40 % τ_o CCCC(S_{99}) + 11 % τ_i CCCC(S_{100})]
415	398	0.1		R1[12 % τ_i CCCC(S_{101})] + R2[29 % τ_i CCCC(S_{105})]

[a] PED <10 % are not included in assignments

[b] Symbols: ν = Stretching, ν_s = Symmetric Stretching, ν_{as} = Asymmetric Stretching, δ = Scissoring, σ = Rocking, τ = Twisting, ρ = Wagging, δ_i = in plane bend, δ_o = out of plane bend, τ_i = in plane torsion, τ_o = out of plane torsion

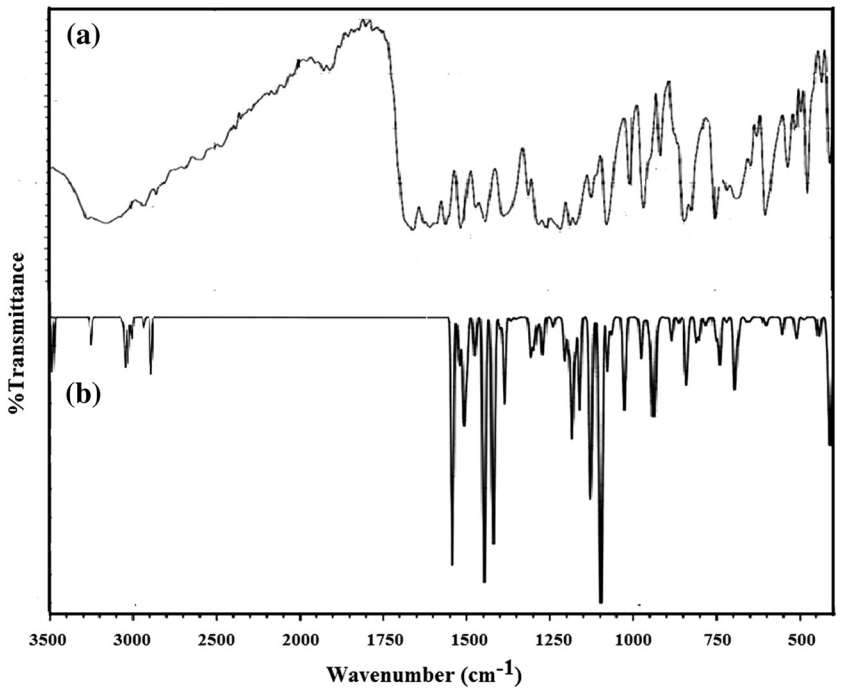

Fig. 3 (**a**) Experimental FTIR and (**b**) simulated IR spectra in the region 3,500–500 cm^{-1}

1,549 cm^{-1} falling in the range of 1,600–1,500 cm^{-1} reported in literature.

The frequencies of in plane and out of plane C–H bending of ring systems are calculated below C–C stretching region. The vibrational mode of strongest intensity calculated at 1,131 cm^{-1} belongs to R3 ring. Rings torsion modes are found in even lower frequency region. A strong and broad band associated to stretching of hydrogen bonded O–H group is observed generally between 3,500 and 3,200 cm^{-1} but it becomes sharp and shifts to higher frequencies in the absence of hydrogen bonding. The calculated value for O–H attached with R3 is 3,551 cm^{-1} much higher than corresponding FTIR value of 3,261 cm^{-1}. It can be attributed to inter-molecular hydrogen bonding present in crystal phase but absent in gas phase of molecule.

N–H stretching vibration with a PED of 100 % is calculated at 3,352 cm^{-1} (Table 2). Furthermore, FTIR value corresponding to this band is 3,157 cm^{-1}. However, in acetohydrazaide molecule (CH_3–CO–NH–NH_2), it is

observed at 3,450 cm^{-1} and calculated at 3,640 cm^{-1} by DFT [41]. The shifting in N–H stretching band in the title molecule is apparently due to hydrogen bonding with oxygen O39 attached with naphthalene ring. The difference in calculated and experimental frequencies of the same indicates that the inter-molecular hydrogen bonding is stronger than intra-molecular H-bond.

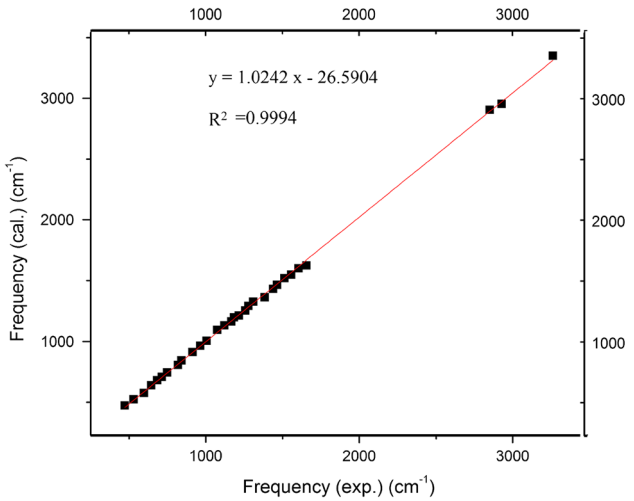

Fig. 4 Correlation between calculated and experimental vibrational frequencies

The stretching of CH_2 is assigned at 2,954 and 2,907 cm^{-1} while bending is seen at 1,467 cm^{-1} both with weak intensities. C–H (attached between N14 and R3) stretching at 2,904 cm^{-1} is one of the bands of strongest intensities. The C = O stretching is reported as a very strong band in the region 1,680–1,640 cm^{-1} [40]. The calculated value 1,625 cm^{-1} and FTIR value 1,656 cm^{-1} agrees with the fact. The C–O stretching in the fragment is found to lie at 991 cm^{-1}. The C–N and C=N stretching coupled with N–H deformation by scissoring and twisting of HCN and HNN respectively are calculated between 1,588 and 1,520 cm^{-1} against reported value of 1,560–1,530 cm^{-1}. However, all these bands are found to be weak instead of intense band reported for acetohydrazide molecule [41]. The calculated frequencies 1,050 and 1,004 cm^{-1} belong to N–N stretching and HCO bending, respectively. The vibrational modes at 1,352 and 680 cm^{-1} are also assigned for bending and deformation of the fragment.

The calculated and experimental frequencies up to 400 cm^{-1} as listed in Table 2 show a close agreement. Figure 4 shows a correlation between these two frequencies. It is apparent that a good correlation exists with a coefficient of 0.9994. This further ensures that the DFT-B3LYP scheme efficiently reproduces the experimental results and can be used for vibrational analysis of biomolecules with a sufficient confidence.

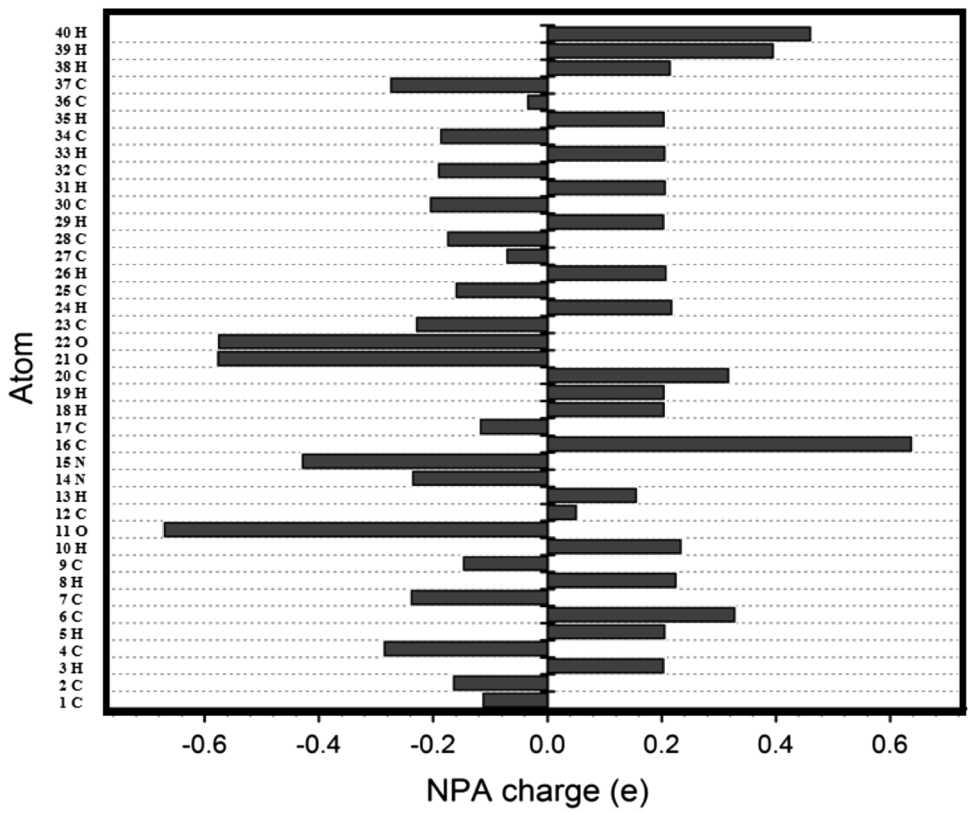

Fig. 5 Partial charges on atoms calculated by NPA scheme at B3LYP/6-311G level

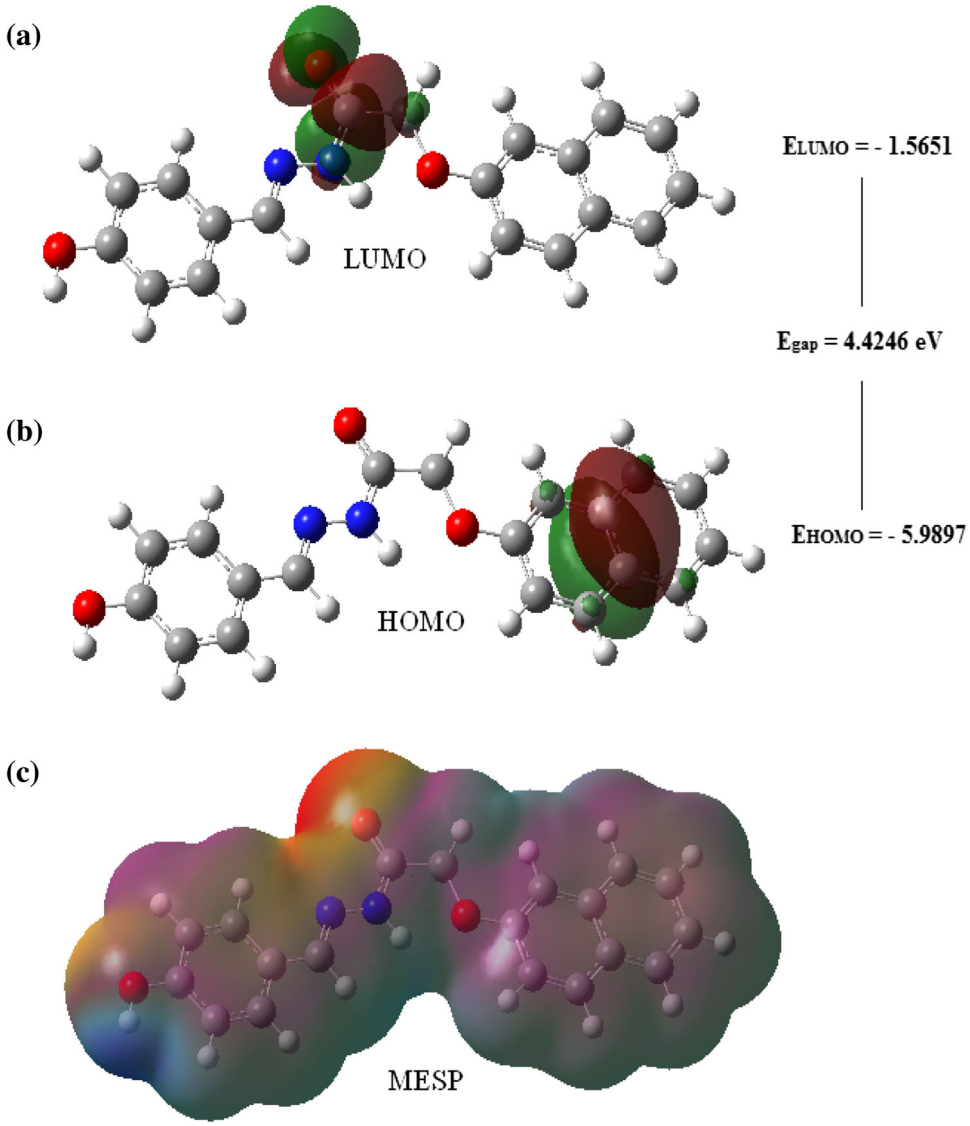

Fig. 6 (**a**) HOMO, (**b**) LUMO and (**c**) MESP plots at B3LYP/6-311G level

3.3. NPA analysis, HOMO–LUMO and MESP plots

Atomic charges of the investigated molecule in gas phase have been computed using NPA scheme at B3LYP/6-311G level. This scheme is more reliable due to its low basis set dependency. The NPA charges range from −0.6699 to 0.6362 e as indicated by bars in Fig. 5. The carbon atoms are found to carry both positive and negative charges. The maximum charge on O11 atom of R3 ring has been seen due to effect of negatively charged oxygen. The nitrogen and oxygen atoms of acetohydrazide fragment, all are negatively charged. Thus, all N and O atoms accept electrons. An increase in charge on N15 as compared to N14 and corresponding decrease in charge on O22 as compared to O21 may be due to electron density transfer from proton donor O22 to proton acceptor N15-H39 involved in hydrogen bonding. It is also interesting to note that charges on hydrogen atoms have only positive values. This clearly explains the charge transfer from H to N, C and O atoms.

The highest occupied molecular orbital (HOMO) represents ability to donate an electron while lowest unoccupied molecular orbital (LUMO) denotes ability to accept it. The HOMO–LUMO plots for studied molecule with corresponding energy values measured from ionization continuum are shown in Fig. 6. Evidently, the HOMO with the energy of −5.9897 eV is located on the naphthalene ring system, while the LUMO with the energy of -1.5651 eV is contributed mainly by acetone group. In acetone group, charges on C16 and O21 are 0.6362 and −0.5767 e, while C27 and C36 of naphthalene carry −0.0702 and −0.0342 e respectively. The transition from HOMO → LUMO indicates charge transfer to acetone group from naphthalene ring. The energy (E_{gap}) between HOMO and LUMO well describes

the chemical reactivity of the molecule. In the present study, this energy gap is found to be 4.4246 eV.

The MESP surface, a map of electrostatic potential on uniform electron density, is used to visualize charge or electron density distribution within the molecule. The importance of MESP lies in the fact that it simultaneously displays molecular size, shape as well as positive, negative and neutral electrostatic potential regions in terms of colour grading (Fig. 6). In the present context, colour code ranges between −0.07753 a.u. for deepest red and +0.07753 a.u. for deepest blue. The electronegative region lies in the vicinity of O21 of acetohydrazide fragment and the most positive one over the hydrogen attached with O11 of R3 ring. On the basis of MESP plot, it can be asserted that an electrophile is attracted towards negative region of acetohydrazide fragment while a nucleophilic attack favours the electropositive region of R3 ring.

3.4. Electronic and thermodynamic properties

Energies of HOMO and LUMO are used to calculate useful global parameters describing chemical reactivity of molecule. These are listed in Table 3. The popular Koopmans' theorem describes ionization potential (I) and electron affinity (A) as the negative of energy eigen values of highest occupied molecular orbital (HOMO) and of LUMO respectively. Other parameters viz. absolute electro-negativity (χ), chemical hardness (η) and electrophilic index (ω) can be found using finite-difference approximations [42]. Dipole moment (μ) of the molecule gives a signature about charge distribution and geometry of the molecule. Electronic energy of investigated molecule is calculated to be −1,068.7645 Hartrees.

The zero point energy (ZPE) and various thermodynamic parameters viz. thermal energy (E), thermal enthalpy (H), thermal free energy (G), constant volume heat capacity (C_v) and entropy (S) are also calculated and listed in Table 3. At room temperature, due to absence of free electrons, electronic contribution is negligible. Translations and rotations share equal but very small contributions. Vibrations, on the other hand, play a crucial role in thermodynamic properties. These parameters are related to one another via standard thermodynamic relations and can be useful for estimation of chemical reaction paths.

Table 3 Electronic and thermodynamic parameters calculated at B3LYP/6-311G

Electronic parameters		Thermodynamic parameters	
I (eV)	5.9897	ZPE (Kcal/mol)	196.850
A (eV)	1.5651	E (Kcal/mol)	209.463
χ (eV)	3.7774	H (Kcal/mol)	210.055
η (eV)	2.2123	G (Kcal/mol)	164.108
ω (eV)	1.4573	C_v (Kcal/mol-K)	78.273
μ (D)	6.0918	S (Kcal/mol-K)	154.109

4. Conclusions

DFT calculations have been carried out on N'-[(E)-4-Hydroxybenzylidene]-2-(naphthalen-2-yloxy) acetohydrazide using B3LYP/6-311G method to perform the structural and vibrational analysis. A good correlation is obtained between experimental and calculated bond lengths and vibrational frequencies. A complete assignment of vibrational modes is presented up to 400 cm^{-1} along with FTIR spectra. The AIM analysis reveals an intra-molecular hydrogen bonding and characterizes it as a weak interaction. The effect of hydrogen bonding on structural as well as vibrational properties is also discussed. NPA analysis, HOMO–LUMO and MESP plots are used to explain chemical reactivity of molecule. Various electronic and thermodynamic parameters have been calculated at the same level of theory which may provide further insights into chemical reactivity and direction of chemical reactions.

Acknowledgments AKS gratefully acknowledges the Council of Scientific and Industrial Research (CSIR), (Grant No. 09/107(0359)/2012-EMR-I) India for providing a research fellowship.

References

[1] A Rauf , M R Banday and R H Mattoo *Acta Chim. Slov.* **55** 448 (2008)
[2] S Rollas, N Gülerman and H Erdeniz *Farmaco* **57** 171 (2002)
[3] V O Kozminykh, A O Belyaev, E V Kozminykh and T F Odegova *Pharm. Chem. J.* **38** 368 (2004)
[4] L W Zheng, L L Wu, B X Zhao, W L Dong and J Y Miao *Bioorg. Med. Chem.* **17** 1957 (2009)
[5] D Sriram, P Yogeeswari and R V Devakaram *Bioorg. Med. Chem.* **14** 3113 (2006)
[6] T L Smalley, et al. *Bioorg. Med. Chem. Lett.* **16** 2091 (2006)
[7] N Raman, S Ravichandran and C Thangaraja *J. Chem. Sci.* **116** 215 (2004)
[8] L Lalib, L A Mohamed and M F Iskander *Transition Met. Chem.* **25** 700 (2002)
[9] M A Affan, I P P Foo, B A Fasihuddin, E U H Sim and M A Hapipah *Malaysian J. Anal. Sci.* **13** 73 (2009)
[10] M Yu, H Lin and H Lin *Indian J. Chem.* **A46** 1437 (2007)
[11] B Szczesna and U Lipkowska *Supramol. Chem.* **13** 247 (2001)
[12] S Vijayakumar , A Adithya , K N Sharafudeen and B K Chandrasekharan *J. Mod J. Mod.Optic.* **57** 670 (2010)
[13] V Singh, V K Srivastava, G Palit and K Shanker *Arzneim-Forsch. Drug. Res.* **42** 993 (1992)
[14] S G Komurcu, S Rollas, M Ulgen, J W Gorrod and A Cevikbas *Boll. Chim. Farm.* **134** 375 (1995)
[15] M Ulgen, B B Durgun, S Rollas and J W Gorrod *Drug Metab. Interact.* **13** 285 (1997)

[16] N N Gulerman, E E Oruc, F Kartal and S Rollas *Eur. J. Drug Metab. Pharmacokinet.* **25** 103 (2000)
[17] S G Kucukguzel, I Kucukguzel and M Ulgen *Farmaco* **55** 624 (2000)
[18] Y Sert, F Ucun and M Böyükata *Indian J. Phys.* **87** 113 (2013)
[19] Y Sert and F Ucun *Indian J. Phys.* **87** 809 (2013)
[20] G A Jeffrey and W Saenger *Hydrogen Bonding in Biological Structures* (Berlin Heidelberg: Springer- Verlag) (1991)
[21] R F W Bader *Atoms in Molecules. A Quantum Theory* (New York: oxford) 2nd ed. (1990)
[22] J Miroslaw and P Marcin *J. Phys. Chem.* **A114** 2240 (2010)
[23] A Nijamudheen, D Jose, A Shine and A Datta *J. Phys. Chem. Lett.* **3** 1493 (2012)
[24] A K Jissy, S Konar and A Datta *Chem. Phys. Chem.* **14** 1219 (2013)
[25] S A Abraham, D Jose and A Datta *Chem. Phys. Chem.* **13** 695 (2012)
[26] M J Frisch, et al. *Gaussian 09 Revision B.01* Gaussian Inc. Wallingford CT (2010)
[27] R Kant, V K Gupta, K Kapoor, S Samshuddin, B Narayana and B K Sarojini *Acta Cryst.* **E68** o2923 (2012)
[28] T A Keith *AIMAll Version 12.09.23* TK Gristmill Software, Overland Park KS USA (2012)
[29] E D Glendening, J K Badenhoop, A E Reed, J E Carpenter and F Weihold *NBO 3.1 Program* Theoretical Chemistry Institute, University of Wisconsin Madison WI (1996)
[30] H J Michal, C D Jan and B Robert *J. Mol. Struct.* **787** 172 (2006)
[31] R Dennington, T Keith and J Millam *GaussView Version 5.0* Semichem Inc. KS (2003)
[32] D R Lide *CRC handbook of Chemisry and Physics* (Boca Raton: CRC Press) 90th ed. (2010)
[33] U Koch and P Popelier *J. Phys. Chem.* **A99** 9747 (1995)
[34] I Rozas, I Alkorta and J Elguero *J. Am. Chem. Soc.* **122** 11154 (2000)
[35] L Rajith, A K Jissy, K G Kumar and A Datta *J. Phys. Chem.* **C15** 21858 (2011)
[36] D Jose and A Datta *Cryst. Growth Des.* **11** 3137 (2011)
[37] E Espinosa, E Molins and C Lecomte *Chem. Phys. Lett*. **285** 170 (1998)
[38] T Steiner *Angew. Chem. Int. Ed.* **41** 48 (2002)
[39] I M Alecu, J Zheng, Y Zhao and D G Truhlar *J. Chem. Theory Comput.* **9** 2872 (2010)
[40] R M Silverstein and F X Webster *Spectrometric Identification of Organic Compounds* (New York: John Wiley and Sons) 6th edition (1998)
[41] H M Badawi *Spectrochim. Acta* **A67** 592 (2007)
[42] R G Parr and W Yang Density Functional Theory of Atoms and Molecules (New York and Oxford: Oxford University Press and Clarendon Press) (1989)